Retinal Vascular Plexuses Are Unequally Affected in Canine Inherited Retinal Degenerations

Ana Ripolles-Garcia,[1] Yineng Chen,[2] Yu Sato,[1] Alexa Gray,[1] Gui-Shuang Ying,[2] Gustavo D. Aguirre,[1] and William A. Beltran[1]

[1]Division of Experimental Retinal Therapies, Department of Clinical Sciences and Advanced Medicine, School of Veterinary Medicine, University of Pennsylvania, Philadelphia, Pennsylvania, United States
[2]Department of Ophthalmology, Scheie Eye Institute, Perelman School of Medicine, University of Pennsylvania, Philadelphia, Pennsylvania, United States

Correspondence: William A. Beltran, School of Veterinary Medicine, University of Pennsylvania, 3900 Delancey Street, Philadelphia, PA 19104, USA;
wbeltran@vet.upenn.edu.

PURPOSE. To characterize the progression of vascular changes that occur in each retinal plexus, in three canine models of inherited retinal degeneration.

METHODS. In this retrospective cohort study, we examined the retinal imaging records of 44 dogs from a research colony that had undergone optical coherence tomography angiography (OCTA) imaging. Animals enrolled included crd2/*NPHP5* and xlpra2/*RPGR* mutant dogs imaged at different stages of photoreceptor loss, as well as RHO$^{T4R/+}$ dogs after acute light-induced rod degeneration. Also included were normal controls imaged at similar ages. OCT angiograms of the superficial vascular plexus combined with the intermediate capillary plexus (SVP + ICP), and the deep capillary plexus (DCP) were analyzed using the AngioTool software to calculate vessel density and other vascular parameters.

RESULTS. A reduction in vessel density was seen over time in both the SVP + ICP and DCP in all mutant dogs but was more pronounced in the DCP. Scans were subclassified based on outer nuclear layer (ONL) thinning compared to age-matched normal controls. When ONL loss was 0% to 50%, vessel density in the DCP was significantly lower than in age-matched controls. In all cases, when ONL loss exceeded 87.5%, vessel density in the SVP + ICP was significantly reduced as well. In the acute light-induced rod degeneration model, the vascular regression changes were observed mainly in the DCP.

CONCLUSIONS. Vessel density reduction in dogs undergoing retinal degeneration is first detected by OCTA in the DCP, and only at later stages in the SVP + ICP.

Keywords: OCTA, retinal vasculature, inherited retinal degeneration, canine, vessel density, vascular plexuses

Inherited retinal degenerations (IRDs) are a genetically and phenotypically heterogeneous group of neurodegenerative diseases that affect humans and several animal species including dogs.[1] Some relevant canine models are the crd2/*NPHP5,* which is the canine homologue to the *NPHP5* form of Leber congenital amaurosis, and the xlpra2/*RPGR* and RHO$^{T4R/+}$, which are non-allelic diseases homologous to different forms of RP.[2–5] Although all IRDs are characterized by the progressive loss of photoreceptors, there are various clinical phenotypes that vary in age of onset, rate of progression and spatial distribution of disease.[1,6] Widespread retinal thinning, attenuation of retinal vasculature, and pallor of the optic disc are common ophthalmic findings in both humans and dogs in advanced stages of IRDs.[7,8]

Photoreceptors are considered to have the highest metabolic rate in the retina, with the majority of their energy being produced in the inner segment.[9–11] The mitochondria located in the inner segment consume oxygen delivered by the choriocapillaris, but those located in the photorecep-

tor's axons are mainly nourished by the retinal vasculature directly, illustrating the dual blood supply of the holangiotic retina.[12,13] As photoreceptors undergo cell death, because of the natural progression of IRDs, there is a steep reduction in oxygen consumption, which in turn causes oxygen from the choriocapillaris to reach the inner retina. This abnormal oxygen diffusion results in a hyperoxic state that in turn reduces the need for oxygen delivery from the inner retinal vessels.[14] It is commonly accepted that it is this abnormal hyperoxic state that triggers the retinal vascular regression seen in IRDs. In other words, the characteristic retinal vascular attenuation seen in IRDs is considered a secondary change occurring after photoreceptor loss.[15,16] By contrast, some argue that the early vascular changes are part of a primary pathological reduction in blood flow that occurs systemically as part of a "vascular dysregulation syndrome" in certain forms of one of the most common IRD, retinitis pigmentosa (RP).[17,18] They consider that this primary vascular regression can worsen the disease course by causing further photoreceptor damage.[17,18]

The holangiotic retinal vasculature in humans, rodents, and dogs consists of four interconnected parallel vascular plexuses: the radial peripapillary capillary plexus located in the nerve fiber layer, the superficial vascular plexus (SVP) in the ganglion cell layer, the intermediate capillary plexus (ICP) in the inner plexiform layer, and the deep capillary plexus (DCP) within the outer plexiform layer. Studies conducted in rodents and humans have suggested that these vascular networks are not equally affected by IRD progression.[19–22] In early stages of disease, the first changes are seen in the DCP, whereas no changes are observed in the vessels of the SVP until advanced stages of degeneration are reached.[21,23–28] Although canine retinas affected by IRDs also undergo vascular thinning and loss, it is currently unknown if there is a selective impairment of the DCP in early stages of degeneration and what the chronology of vascular changes with disease progression is.

Optical coherence tomography angiography (OCTA), a functional extension of OCT technology, enables in vivo assessment of the different vascular networks as separate en face images as opposed to single full-retinal thickness en face angiograms rendered in dye-based imaging procedures, such as fluorescein angiography.[25,29,30] OCTA images from the different retinal plexuses in IRD patients have enabled the detection and quantification of the extent of vasculature loss that occurs with disease progression.[22,31] In several OCTA studies conducted in human RP patients and rodents, the most prominent vascular regression was found in the DCP.[21,22,32–34] This is in contrast with other reports that have shown in RP patients a vascular impairment and reduced vessel density in both the SVP and DCP.[32,35–39] Noteworthy, the cross-sectional nature of the studies and the lack of categorization based on disease stage prevented drawing final conclusions regarding which plexus is affected more severely or earlier. OCTA technology has been recently validated in dogs for imaging and quantifying individual vascular plexuses,[25,29] but it is currently unknown if a differential impairment of specific retinal plexuses occurs in canine IRDs.

The aim of this study retrospective was to characterize the changes in vascular density, as measured by OCTA, that occur in the main vascular networks of the cone-rich area centralis centered on the fovea-like region[28] in two canine models of IRDs: crd2/*NPHP5* and xlpra2/*RPGR*. We also evaluated the vascular changes in a model of light-induced acute retinal degeneration (RHO$^{T4R/+}$) and in a crd2/*NPHP5* mutant dog that had been treated by gene therapy (GT). Additionally, we complemented the in vivo evaluation with histopathologic characterization of the vascular structural changes that accompany retinal degeneration.

MATERIALS AND METHODS

Study Animals

The animals evaluated were part of a research colony maintained at the University of Pennsylvania, Retinal Diseases Studies Facility. All the procedures were carried out in strict accordance with the ARVO Statement for the Use of Animals in Ophthalmic and Vision Research and approved by the Institutional Animal Care and Use Committee of the University of Pennsylvania (IACUC no. 804956).

Retinal imaging records of dogs that had undergone OCTA imaging were reviewed. Inclusion criteria were (1) confirmed IRD genotype and (2) quality of the OCTA images above 40 dB (10° × 10° acquired at the area centralis) in at least one eye and one time-point. A total of 44 dogs were enrolled; this included 16 crd2/*NPHP5*, 11 xlpra2/*RPGR* and 3 RHO$^{T4R/+}$ mutant dogs, as well as 14 normal controls of different ages and with both genders represented (see Supplementary Table S2).

As a proof of concept, one animal that had been previously enrolled in AAV-mediated GT studies unrelated to this project (ID: AS2-439) underwent OCTA imaging 81, 108, and 137 weeks after administration of the viral vector product in one eye.[40] This animal received the GT as a subretinal injection only in the left eye at mid-stage disease (13.2 weeks). The right eye was injected with balanced salt solution to be used as a control of the GT effect, and to study the natural progression of the disease.

In the RHO$^{T4R/+}$ model of autosomal dominant RP, when the heterozygous or homozygous affected animals are maintained from birth in a protective dim red-light environment, their retinal structure remains intact and comparable to that of normals.[41,42] However, acute retinal degeneration can be triggered experimentally if the eyes are exposed to white light.[42] The three RHO$^{T4R/+}$ mutants had their left eye exposed for one minute (intensity of corneal irradiance of 1 mW/cm^2) of white light following a pre-established protocol.[42] Two weeks after light exposure, the retinal structure was assessed in vivo by OCT and OCTA in both eyes. The results of the imaging at this timepoint were compared to those obtained immediately before light exposure and to those of age-matched normal controls.

OCT and OCTA Imaging Acquisition

Animal preparation and acquisition of OCTA images under general anesthesia were performed as previously validated by our group, using a cSLO/OCT unit (OCTA module, Spectralis HRA+OCT2, version 6.9.4.0, Heidelberg Engineering Inc., Heidelberg, Germany).[25] The vasculature was characterized at different ages, by acquiring a 10° × 10° OCTA scan at the center of the area centralis, the canine analog of the human foveo-macular area.[28] Because the vascular parameters vary depending on the retinal topography,[25] the fovea-like region at the center of the area centralis was selected for maximal consistency across animals and ages. This region was accurately identified following landmarks such as the vascular pattern around it and the orientation of the nerve fiber layer.[25,28] Each 10° × 10° scan was composed of 512 B-scans (ART mode was set at seven frames per scan in all OCT-A examinations) with a nominal spacing of 6 μm. The C-scan (en face) visualization of this OCT-A was automatically derived from the OCT B-scan angiograms as mentioned above. One of the main advantages of the Spectralis OCTA unit is the ability to image longitudinally the exact same area of the retina by selecting follow-up scans.[25] We used this feature to characterize longitudinally the vascular changes in mutant animals (see Supplementary Table S2).

The ONL thickness was measured on the OCTA B-scan as previously described using the Heyex Software (Version 1.9.201.0; Heidelberg Engineering, Heidelberg, Germany).[25] For each measurement, the result from three areas separated by 0.5 mm at the center of the area centralis were averaged. Angiograms from the SVP combined with the ICP (SVP + ICP), and the DCP were extracted based on the recently characterized OCT localization of the canine retinal plexuses.[25] An important inclusion criterion for the OCTA images was that they be of acceptable quality (signal-to-noise ratio

provided by HEYEX Spectralis software >40dB; range: 20-53 dB). We excluded all OCTA images that had visible artefacts (mainly motion artefacts and decorrelation abnormalities caused by projection artefact). A low signal-to-noise ratio was frequently seen in advanced disease stages because of cataract formation or vitreal degeneration that often are secondary to the retinal degeneration.

Vascular Network Quantification by AngioTool

For each eye, OCT angiograms from the SVP+ICP and the DCP were analyzed using AngioTool, as previously described.[25,43] The parameters selected in our evaluation were vessel thickness of at least 5 μm, vessel pixel intensity of 15–255 and the options "Remove small particles" and "Fill holes" were selected. For each analyzed slab, we selected among the AngioTool parameters: vessel density, Junction Density, Average Vessels Length, and Lacunarity. The axial globe length was measured after each imaging session by ultrasound (Sonomed A-scan A1500, Sonomed-Escalon, Lake Success, NY, USA). We calculated the retinal magnification factor (expressed in mm/deg) based on the individual axial globe length (in mm) and the following formula retinal magnification factor = $2*\pi*(0.59*$ axial globe length)/360, as previously described for correcting for curvature bias.[28] By using this simplified model, we were able to convert length measurements expressed in degrees into values expressed in μm units. Then, we used the AngioTool software to calibrate de measurements based on the pixel and the μm size of each image. Therefore the exact area covered by the 10° × 10° scan for each eye was used to calibrate the AngioTool software and obtain accurate quantifications.

Vascular Remodeling Evaluation by Immunohistochemistry and Confocal Imaging

For histological characterization of the vascular alterations that occur with progressive retinal atrophy, frozen paraformaldehyde-fixed retinal archival tissues from mutant animals were evaluated. The tissues were processed as previously described.[25] These included tissue blocks from 13 crd2/*NPHP5*- and 11 xlpra2/*RPGR*-affected animals at several ages representing different stages of retinal degeneration. It should be noted that these animals were not the same than the ones imaged by OCTA.

The samples had previously been stored frozen embedded in optimal cutting temperature media. For evaluation of the retinal vasculature, the tissues were thawed in phosphate balanced solution overnight, and the embedding media was removed. The neuroretina was separated and incubated for four days at 4°C in a solution containing a mixture of two primary antibodies that labeled the von Willebrand factor located in in the vascular endothelium[44] (1:400; Dako A0082, Carpinteria, CA, USA) and the collagen type IV present in the basal lamina[45] of the retinal vessels (1:100, Millipore Sigma AB769, Burlington, MA).[25] Selected neuroretinas were also incubated in a solution containing primary antibodies against RPE65 protein (1:500, Novus Biologicals 401.8B11.3D9, Englewood, CO). Fluorochrome-labeled secondary antibodies (Alexa Fluor 488, 568 and 647 dyes; 1:200, Thermo Fisher Scientific, Waltham, MA, USA) and DAPI nuclear stain were applied for 24 hours at 4°C.

The retinal tissues were imaged using a 2-photon confocal microscope (Leica SP8 Multiphoton; Leica Microsystems, Wetzlar, Germany) with a 20× (HCX APO L, 1.0 NA) water immersion objective lens. The captured images were composed of individual 0.5 mm² fields, acquired from z stacks spanning the inner limiting membrane (ILM) to ONL. Z-stacks were acquired at 0.5 μm Z-steps in 1024 × 1024 pixel format at 400 Hz with a line average of 2. These settings offered a lateral resolution of 0.541 μm/pixel and axial resolution of 0.5 μm/pixel. Several individual images were acquired to cover a 2 mm square area centered in the area centralis. In the crd2/*NPHP5* dogs, a comparative area in the nasal quadrant, centered at the visual streak was used instead because of the unavailability of that bloc of tissue that was being used for GT studies. The images were merged and qualitatively evaluated using the Leica Application Suite (LAS X, 3D Visualization Module). The angiograms from the SVP + ICP and DCP were extracted and further analyzed with AngioTool software following the same steps previously mentioned for OCTA images.[25]

Data Processing and Statistical Analyses

The data was imported, analyzed, and plotted using excel spreadsheets (Microsoft Excel, version 2019) and R software (version 4.1.1; R Foundation for Statistical Computing, Vienna, Austria) with the correspondent built-in packages.[46] The ggplot2 package in R was used for OCTA data visualization (version 3.3.5., Wickham, 2016).[47] All statistical analyses were performed using SAS v9.4 (SAS Institute, Cary, NC, USA) and two-sided $P \le 0.05$ was considered statistically significant.

Because all the animals had OCTA images acquired in both eyes, we evaluated the inter-eye agreement for each OCTA parameter (ONL, vessel density, junction density, average vessel length, and lacunarity) using the intra-class correlation and its 95% confidence interval (CI) (Supplementary Table S1). Because the intra-class correlation was only moderate for most of the OCTA parameters, we used data from each individual eye for downstream analysis and the inter-eye correlation was accounted for by using generalized estimating equations (GEE).

The analysis of OCTA and histology parameters comparing the study groups and age-matched controls were performed using a generalized linear model, and the GEE with compound symmetry covariance was used to account for the inter-eye correlation and repeated measures correlation.

The Pearson's correlation coefficient was used to evaluate the correlation between the vessel density in the SVP + ICP and vessel density in the DCP with the ONL thickness. For each plexus and study group, we fitted a linear or quadratic model based to visualization of the data distribution in a scatterplot and the *P* value from statistical tests for the evaluation of the significance of a quadratic term. The linear regression model only contained the ONL thickness as the predictor, whereas the quadratic model contained both ONL thickness and square of ONL thickness as predictors. The Pearson's correlation coefficient was calculated as the correlation between predicted vessel parameter (based on linear or quadratic model) and observed vessel parameter. The correlation coefficient was interpreted as follows: R = 0.00–0.10, negligible correlation; R = 0.10–0.39, weak correlation; R = 0.40–0.69, moderate correlation; R = 0.70–0.89, strong correlation; R = 0.90–1.00, very strong correlation.

RESULTS

OCT Angiograms Reveal Selective Impairment of the DCP

To characterize longitudinally the retinal vascular changes occurring with disease and compare them to normal, the OCT (ONL thickness) and OCTA parameters evaluated (vessel density in the SVP + ICP and DCP) were plotted as a function of age (Figs. 1A, 1B). As the disease progressed, the ONL became thinner, reflecting a progressive loss of photoreceptors and their nuclei (Fig. 1A). Vessel density in the SVP + ICP decreased over time in all dogs, ;however, the values were slightly lower in mutant animals (Fig. 1B1). Vessel density in the DCP remained stable in the normal dogs but showed a marked decline in the mutants (Fig. 1B2). This initial overview of the dataset already suggested that in IRD dogs, the DCP is more affected and at an earlier stage than the SVP + ICP.

Evaluation of vascular changes based only on the age of the mutant animals, does not take into consideration the fact that these different models vary in their temporal course of disease (different age of onset and kinetics of photoreceptor loss).[2,48,49] Therefore, to provide a more accurate analysis, we classified each datapoint based on the ONL thickness in the mutant animals compared to that of age-matched normal animals (Figs. 1C1, 1C2). This allowed us to compare the vascular parameters across disease models based on the stage of degeneration by defining four quantitative stages of ONL thickness loss: 0%-50%, 50%-75%, 75%–87.5%, and 87.5%–100%. When evaluating the OCTA images, the vessels from both the superficial and deep networks were affected with disease progression, although the DCP seemed to be affected at an earlier disease stage (Fig. 2). In both models when ONL thickness loss was between 50% to 75%, no major vascular remodeling was detected in the SVP + ICP (Figs. 2A1, 2B1); however, subtle changes and multi-
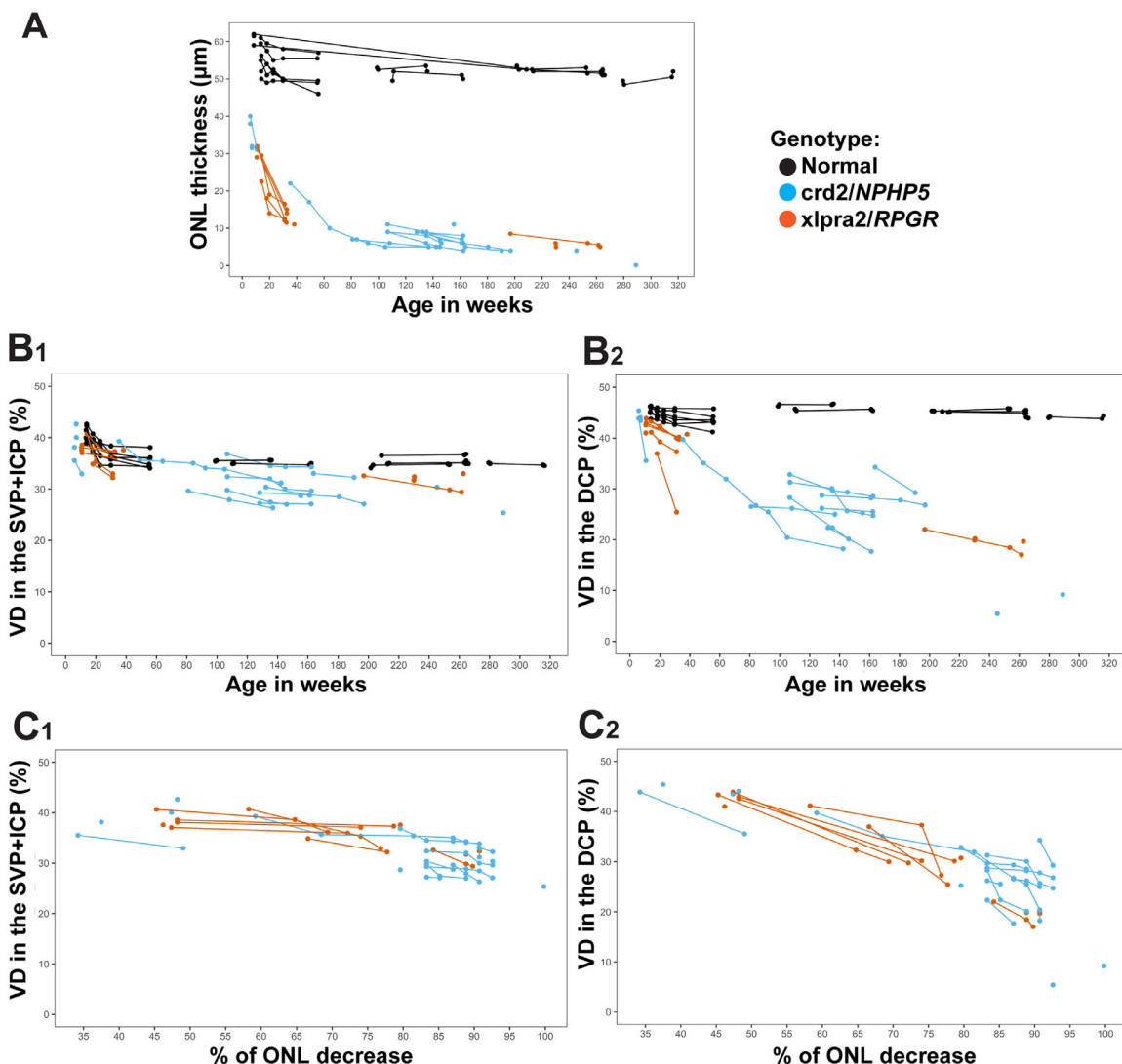

FIGURE 1. Longitudinal measurements of ONL thickness, vessel density in the SVP+ICP and vessel density in the DCP in normal and mutant animals [normal (n = 14), crd2/*NPHP5* (n = 16), and xlpra2/*RPGR* (n = 11)]. (**A**) Scatter plot of mean ONL thickness at different ages in normal and mutant animals. (**B1-2**) Scatter plot of mean vessel density in the SVP+ICP and DCP at different ages in normal and mutant animals. (**C1-2**) Scatter plot of mean vessel density in the SVP+ICP and DCP at different percentages of ONL decrease when compared to normal, in mutant animals. Datapoints from the same animals are connected with a *solid line*. VD, vessel density.
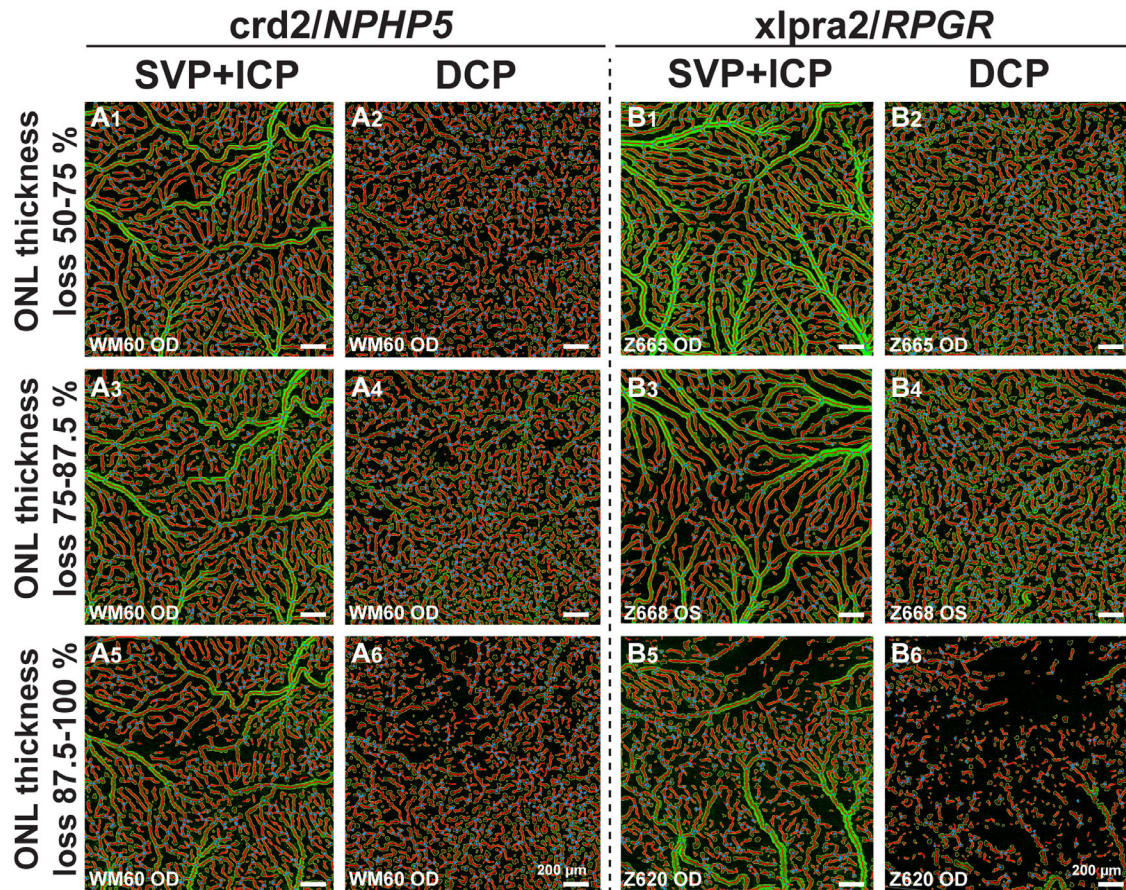
FIGURE 2. Representative OCTA images processed with AngioTool of the SVP+ICP and DCP vascular networks at different stages of disease in the mutant animals. Representative images from crd2/*NPHP5* (**A**) and xlpra2/*RPGR* (**B**) mutant animals for the SVP+ICP and DCP. The mutant animals were subclassified based on their ONL thickness loss, to illustrate the changes when there was a ONL loss of 50% to 75% (panels 1, 2), 75% to 87.5% (panels 3, 4), and 87.5% to 100% (panels 5, 6). OD, right eye; OS, left eye. See Supplementary Figure S1 for an illustration of the vascular skeletonization with AngioTool in normal retinas.

focal loss of the continuity in the DCP could be identified (Figs. 2A2, 2B2). See Supplementary Figure S1 for images illustrating the AngioTool vascular skeletonization pattern in three normal dogs.

Quantitative comparisons at different stages of ONL thickness loss showed that, when the loss was between 50% and 75%, the vessel density in the SVP+ICP of crd2/*NPHP5* was mildly yet significantly increased compared to the vessel density in the same plexus in age-matched controls (Supplementary Table S3 and Fig. 3A1). In the same animals, the vessel density in the DCP was significantly reduced at an earlier disease stage, when the ONL thinning was between 0% and 50% (Supplementary Table S3, Fig. 3A2). In xlpra2/*RPGR* mutants, a significant reduction in vessel density of the SVP + ICP was only seen with severe ONL loss (87.5%-100%) (Supplementary Table S4, Fig. 3B1), but significant reduction in vessel density of the DCP was seen at all stages of retinal degeneration (Supplementary Table S4, Fig. 3B2), showing that the DCP is more severely affected at an earlier disease stage.

The other vascular structural parameters evaluated (junction density, average vessel length and lacunarity) also showed abnormalities. Overall, the junction density followed a similar pattern to that seen with vessel density, where there was a decrease over time in both the SVP+ICP (Supple-

mentary Tables S3, S4, Supplementary Figs. S2A1, S2B1) and the DCP (Supplementary Tables S3, S4, Supplementary Figs. S2A2, S2B2). The magnitude of the reduction was more marked in the DCP. In all the mutants, the most pronounced increase in average vessel length in the SVP + ICP was seen in the first stage of disease (Supplementary Tables S3, S4, Supplementary Figs. S3A1, S3B1), but there was a decreased average vessel length in the DCP over time (Supplementary Tables S3, S4, Supplementary Figs. S3A2, S3B2) that qualitatively corresponded with decreased tortuosity of the capillaries. The lacunarity increased in all the mutants evaluated with significant changes seen in both the SVP + ICP (Supplementary Table S3, S4, Supplementary Figs. S4A1, S4B1) and the DCP (Supplementary Tables S3, S4, Supplementary Figs. S4A2, S4B2), reflecting a decrease in homogeneity in these vascular networks as the disease progressed.

The Vessel Density in the DCP by OCTA Shows a Stronger Correlation With ONL Thickness Than Vessel Density in the SVP + ICP

After visualizing with scatter plots the relationships between the vessel density in the SVP + ICP and the vessel density in the DCP with the ONL thickness, we fitted the data from
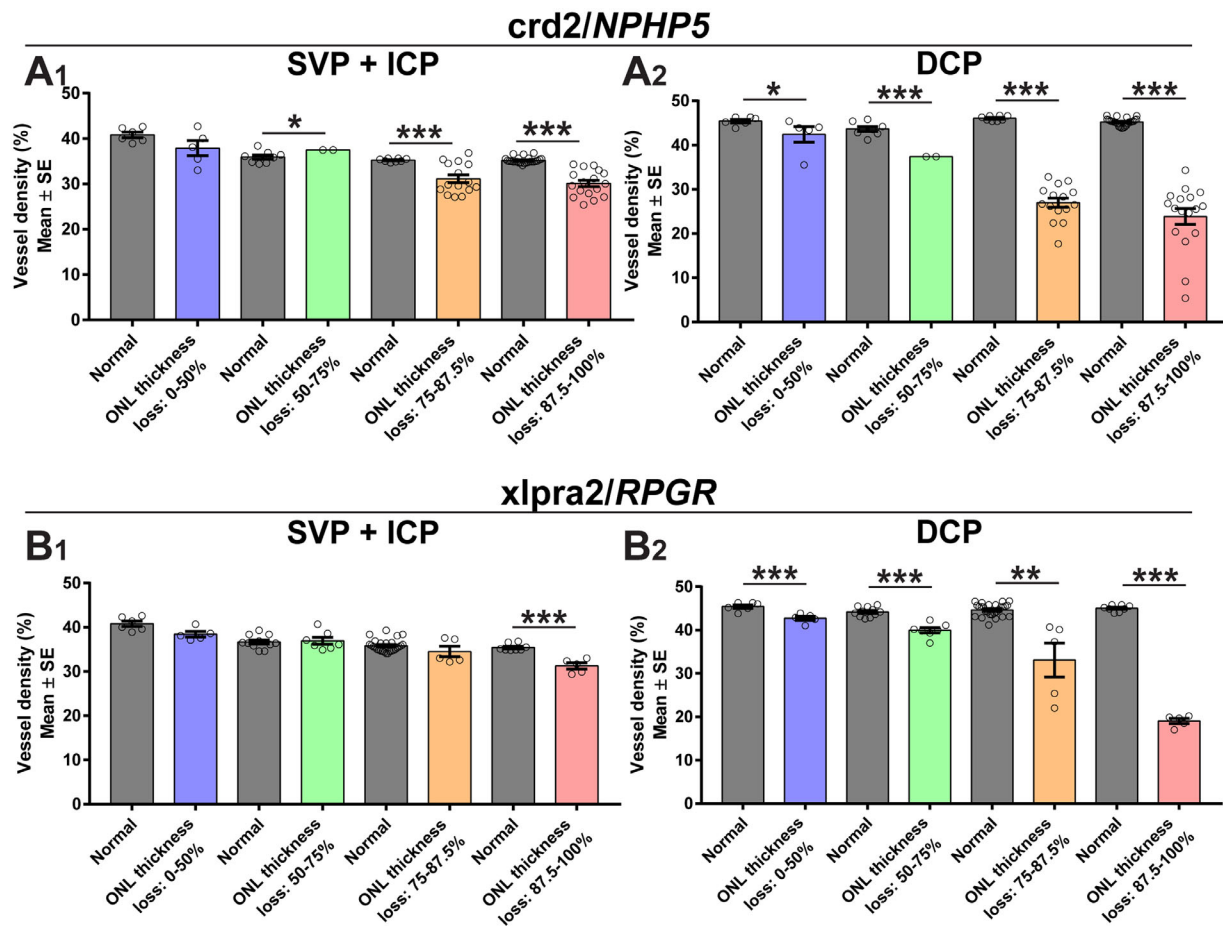
FIGURE 3. Vessel density (mean ± SE) from OCTA images of the SVP + ICP and DCP vascular networks, obtained in mutant animals at different disease stages. Vessel density values of the SVP+ICP (**A1, B1**) and DCP (**A2, B2**) are shown for the crd2/*NPHP5* (**A**) and xlpra2/*RPGR* (**B**) mutants. Each group is compared to an age-matched subgroup of normal dogs. VD, vessel density. GEE model: *$P \leq 0.05$, **$P \leq 0.01$, ***$P \leq 0.001$.

TABLE. Correlation Between Outer Nuclear Layer Thickness and Vessel Density in the Superficial (SVP + ICP) and DCP Vascular Networks in Two Canine Models of Inherited Retinal Degeneration and Normal Dogs

	Pearson's Coefficient R (95% CI)	
	SVP + ICP	**DCP**
crd2/*NPHP5*	Linear model: 0.70 (0.53, 0.87)	Quadratic model: 0.83 (0.69, 0.93)
xlpra2/*RPGR*	Quadratic model: 0.70 (0.50, 0.86)	Quadratic model: 0.91 (0.77, 0.97)
Normal	Linear model: 0.45 (0.11, 0.73)	Linear model: 0.41 (0.08, 0.62)

The inter-eye correlation and repeated measures correlation was considered using bootstrap for 95% CI. The correlation coefficient was interpreted as follows: R = 0.00–0.10, negligible correlation; R = 0.10–0.39, weak correlation; R = 0.40–0.69, moderate correlation; R = 0.70–0.89, strong correlation; R = 0.90–1.00, very strong correlation.

each group into linear and quadratic regression models to determine which one better described their relationships (Supplementary Fig. S5, Supplementary Table S5). In the crd2/*NPHP5* retinas, the correlation between the vessel density in the SVP+ICP and the ONL thickness was best fit by a linear model ($R^2 = 0.49$), whereas for the correlation between DCP and ONL thickness a quadratic model provided a better fit ($R^2 = 0.70$, $P = 0.02$ for the quadratic term; Supplementary Table S5). On the other hand, in the xlpra2/*RPGR* retinas, the correlation of vessel density in the SVP + ICP and DCP with ONL thickness was best fit with a quadratic model, (Supplementary Table S5). Last, in the

normal dogs, both correlations were better explained by a linear model (Supplementary Table S5). In the absence of OCTA data, these mathematical models could offer the possibility of estimating the vessel density based on ONL thickness measurements only.

When evaluating the strength of these correlations in the mutant animals, we observed that the association between vessel density in the DCP and ONL thickness was stronger than that seen between vessel density in SVP + ICP and ONL thickness (Table). The correlation between the vessel density in the DCP with the ONL was in all cases strong/very strong and higher than that of the SVP + ICP (Table). In contrast,
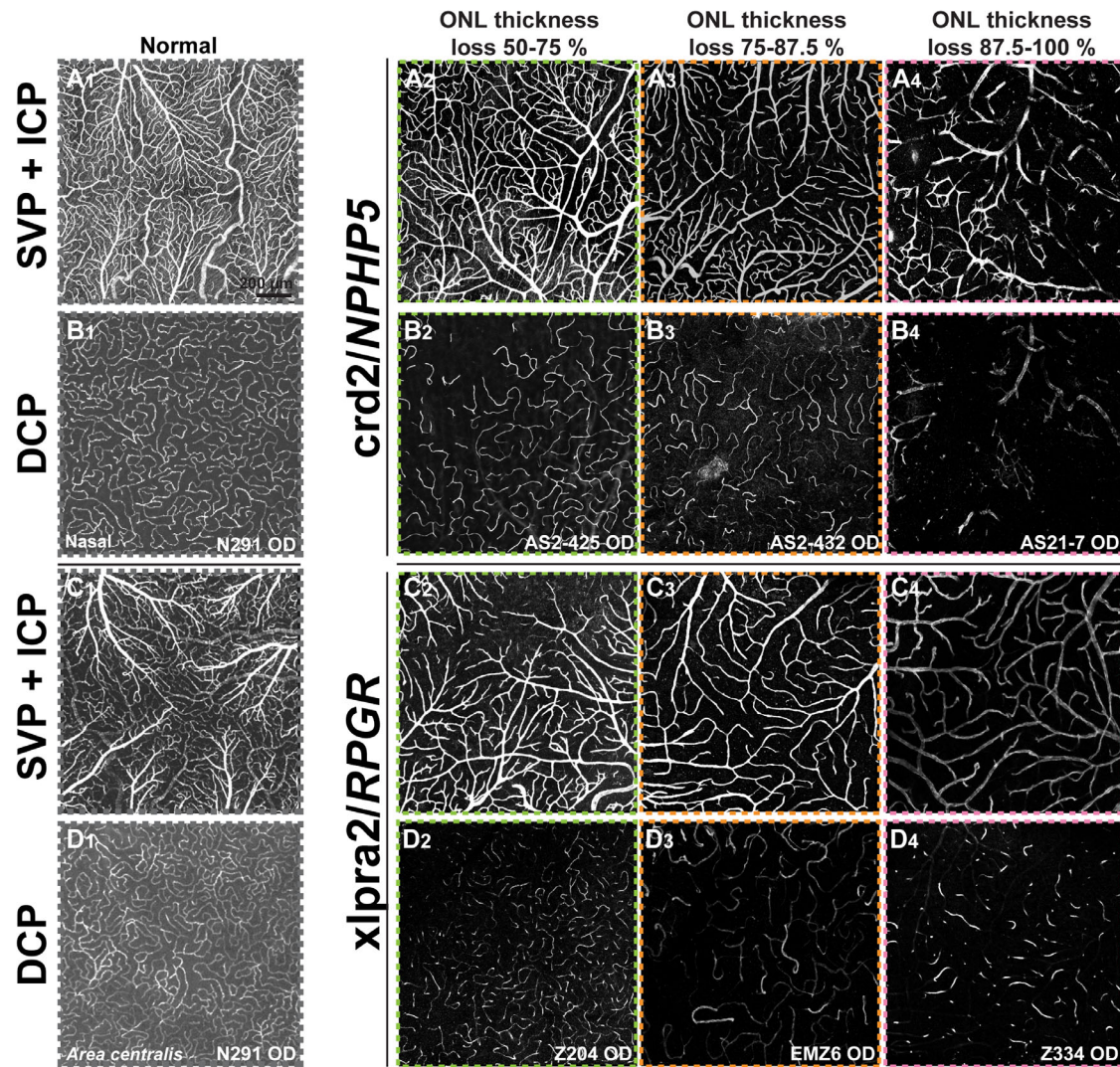
FIGURE 4. Illustration of the vascular networks in mutant dogs at different stages of disease, imaged by immunohistochemistry and confocal microscopy of retinal flat mounts. (**A, B**) Representative images of the SVP+ICP (**A2–A4**) and DCP (**B2–B4**) in crd2/*NPH5* dogs. (**C, D**) Representative images of the SVP+ICP (**C2–C4**) and DCP (**D2–D4**) in xlpra2/*RPGR* dogs. The animals were subclassified based on their ONL thickness loss, to illustrate the changes when there was a ONL loss of 50%–75% (panel 2), 75%–87.5% (panel 3), and 87.5%–100% (panel 4). (**A1, B1, C1, D1**) Illustrations of the normal vasculature in the areas studied for comparison purpose. OD, right eye; OS, left eye.

the correlation between the vessel density in the SVP + ICP and the ONL thickness was moderate (Table). Interestingly, in the normal animals, the correlations between ONL thickness and vessel density in the SVP + ICP and DCP were comparable (Table) suggesting that the outer retinal diseases have different and possibly independent effects of the different plexuses with disease progression.

Evaluation of Vasculature in Retinal Flat Mounts Confirms Earlier and More Severe Alterations in the DCP With Disease Progression

We evaluated the vascular alterations across different disease stages based on ONL thinning by confocal microscopy on retinal flat mounts and compared the findings to those of normal dogs (Figs. 4A1, 4B1, 4C1, 4D1). When the ONL thickness loss was between 50%–75%, the only noticeable changes in the SVP + ICP was minor loss of the small-est vessels (Figs. 4A2, 4C2). However, in both models, the earliest appreciable change was marked thinning of the DCP capillaries (Figs. 4B2, 4D2). When the ONL thinning was between 75% to 87.5%, the loss of capillaries from the SVP + ICP was more pronounced (Figs. 4A3, 4C3). At this stage, the DCP was reduced from being a continuous network to retaining only multifocal loops extending from the ICP (Figs. 4B3, 4D3). Morphologically, the vessels in the abnormal DCP were less tortuous and more spaced than at previous timepoints or in normal dogs. Lastly, in end stage disease (ONL thickness loss of 87.5%-100%), only the SVP was present in most animals, but vessels had a pronounced narrowing of their lumen (Figs. 4A4, 4C4).

When comparing quantitatively the vessel density of the retinal plexuses of retinal flat mounts imaged by confocal microscopy over time, we observed a similar trend to that of the OCTA data: the vessel density in the SVP + ICP did not significantly decrease until advanced stages of degeneration were reached (Supplementary Figs. S6A1, S6B1, Supplemen-
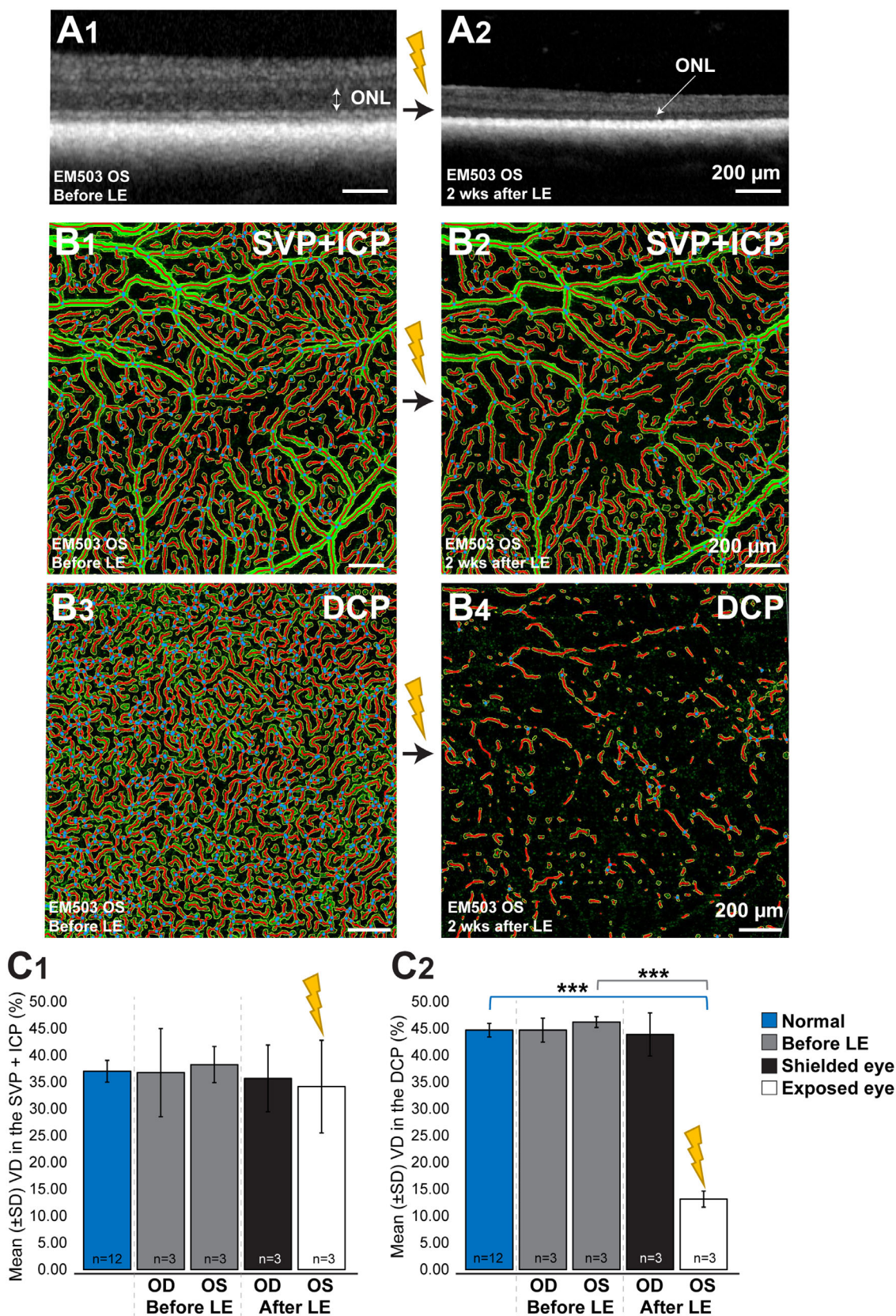
FIGURE 5. Changes in the vascular plexuses after acute light-induced retinal degeneration in the RHO$^{T4R/+}$ mutant. (**A**) OCT b-scans, which denote the ONL before (**A1**) and two weeks after the light exposure (**A2**). (**B**) OCTA images processed with AngioTool of the SVP+ICP before (**B1**) and two weeks after the light exposure (**B2**), as well as the DCP before (**B3**) and two weeks after the light exposure (**B4**). (**C**) Quantification of the vessel density (mean ± SE) in the SVP+ICP (**C1**) and DCP before and two weeks after light exposure in the left eye (**C2**). Paired t-test: *$P \leq 0.05$, **$P \leq 0.01$, ***$P \leq 0.001$. OD, right eye; OS, left eye; LE, light exposure.
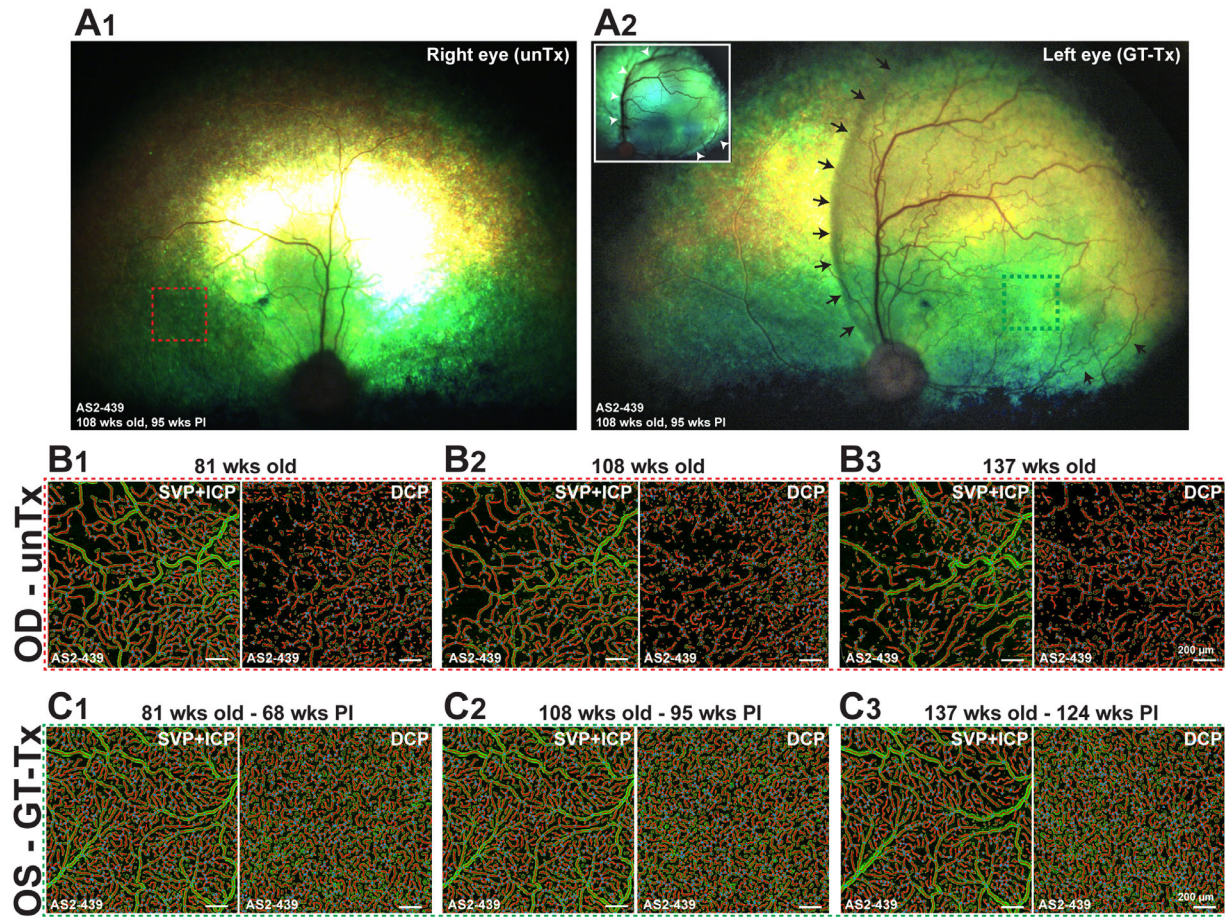
FIGURE 6. Illustration of the vascular preservation achieved with NPHP5 gene augmentation therapy in crd2/*NPHP5* mutant. (**A1**) Fundus photograph of the untreated eye. (**A2**) Fundus photograph of the subretinally-treated eye at 95 weeks post injection. Black arrows demarcate the treated area. **Insert:** *white arrowheads* point to the border of the subretinal bleb, immediately after injection. (**B**) Illustration of OCTA images processed with AngioTool in the untreated eye at 81 (**B1**), 108 (**B2**), and 137 (**B3**) weeks of age. (**C**) Illustration of OCTA images processed with AngioTool in the treated eye at 68 weeks after treatment (81 weeks of age, **C1**), 95 weeks after treatment (108 weeks of age, **C2**), and 124 weeks after treatment (137 weeks of age, (**C3**). unTx, untreated; GT-Tx, gene therapy treated; OD, right eye; OS, left eye; PI, post-injection.

tary Table S6). On the other hand, the vessel density in the DCP was significantly reduced at an earlier stage in both canine models (Supplementary Figs. S6A2, S6B2, Supplementary Table S6).

Last, we found that the microscopic vascular changes associated with degeneration were different in the various retinal networks. In the DCP, a progressive narrowing and reduction to only few loops, ending in complete disappearance of this network was confirmed (Supplementary Figs. S7A1–S7A4). Interestingly, a particular vascular complex was seen throughout the degenerated retinas (Supplementary Figs. S7B1–S7B2, Supplementary Video S1), characterized by vessels being pulled toward the center of this abnormal vascular feature. In these areas, the vessels from the SVP were seen invaginating deeper into the outer retina (Supplementary Fig. S7B2). The number of vascular complexes was higher in the crd2/*NPHP5* retinas than in the xlpra2/*RPGR* models. In the SVP of both models, we observed extensive areas where endothelial cells were absent from the vascular lumen (Supplementary Fig. S7C1). After endothelial cell loss in this plexus, the vascular structure remained as acellular ghost vessels staining only with collagen type IV (Supplementary Fig. S7C1) but with no nuclear staining associated

with them. There was perivascular deposition of material that led to vascular narrowing and occlusion (Supplementary Figs. S7C2, S7C3). At end-stage disease, multiple vessels from the SVP were found to be surrounded by pigmented structures (Supplementary Figs. S7D1, S7D2). In areas of the canine tapetal fundus where the retinal pigmented epithelium (RPE) is non-pigmented, RPE65 immunolabeling confirmed that these were RPE cells that had migrated and surrounded the inner retinal vessels (Supplementary Figs. S7D3, S7D4, Supplementary Video S1). Moreover, even though no overt pigmentation was seen associated with the above-mentioned vascular complexes, specific labeling of RPE cells also identified their involvement in these structures (Supplementary Figs. S7D5, S7D6, Supplementary Video S1).

Acute Light-Induced Retinal Degeneration in RHO^{T4R/+} Dogs Affects Primarily the DCP

OCT and OCTA imaging conducted prior to light-induced retinal degeneration in RHO^{T4R/+} dogs confirmed that their retinal structure/lamination and vascular network was normal (Figs. 5A1, 5B1, 5B3). However, two weeks after the

one-minute light-exposure (corneal irradiance of 1 mW/cm^2) that does not damage the normal retina,[42] there was a drastic loss of ONL thickness when compared to baseline (Fig. 5A2) accompanied by remodeling of the vascular networks, particularly in the DCP (Fig. 5B4). The images were then analyzed using AngioTool and compared to normal age-matched controls. To assess the extent of the retinal degeneration achieved after light exposure, we measured the ONL thickness and found a 94.36% decrease compared to baseline. The vessel density in the SVP + ICP was decreased by 10.74% (Fig. 5C1) and 44.71% in the DCP (Fig. 5C2). When comparing the vessel density in DCP, we found that there was a significant decrease when compared to normal ($P = 0.001$; Supplementary Table S7) and baseline values ($P = 0.001$; Supplementary Table S7). However, no significant differences were found when comparing the vessel density in the SVP + ICP after light exposure with that of normal dogs ($P = 0.57$; Supplementary Table S7) and baseline value ($P = 0.12$; Supplementary Table S7) emphasizing the unique sensitivity of the DCP to outer retinal damage.

Gene Therapy Preserves the Vascular Integrity in Parallel With Retinal Structure

In the unilaterally crd2/*NPHP5* GT-treated animal whose subretinal injection covered the area centralis and was included in the OCTA evaluation, the ONL loss at the time of GT intervention was less than 50%. When comparing fundus photographs from the untreated (Fig. 6A1) and treated eyes (Fig. 6A2), a marked preservation of the vasculature in the area that was covered by the GT was readily identified (Fig. 5A2). The OCTA images were processed with AngioTool, and qualitative assessment of the skeletonized images showed vascular regression in the untreated eye (Figs. 5B1–5B3) and a remarkable preservation of vascular integrity in the treated eye (Figs. 5C1–5C3).

DISCUSSION

In this study, we evaluated the vascular changes in the area centralis of dogs affected by several forms of IRD that were imaged by OCTA at different disease stages. We identified that the DCP is more severely affected than the more superficial vascular networks at early-stage disease. Moreover, we confirmed that there is a strong association between the vessel density in the DCP and the ONL thickness, which suggests that evaluation of the vasculature in this plexus can be used as a surrogate marker for assessment of the metabolic requirements of the outer retina.[20] We also validated by analysis of vessels in retinal flat mounts the OCTA findings and found that in canine models of IRD, migration of RPE cells also plays a role in the later stage vascular alterations that occur in RP patients.[50]

In patients affected by IRDs, several studies have shown choroidal and retinal vascular impairment using OCTA.[21,31,39,51] However, there is controversy on the vascular plexuses that are altered. Some reports state that both plexuses are affected,[31,32,35–39,52] whereas others show significant differences only in the DCP.[19–21,24,27,53] Differences in OCTA instruments, study design and methodologies used might explain some of these disparities, as well as variabilities in disease staging or the causal gene/mutation involved. Noteworthy, these studies did not report their findings based on the stage of degeneration, which precluded

identifying the chronological changes that occur in the different plexuses.[54–56] Our results are in strong concordance with those studies that identified alterations mostly in the DCP at earlier stages of degeneration.[21,24,27,34]

Additionally, we observed that in degenerating retinas, the capillaries became straighter. This loss of tortuosity has been previously identified as an early sign of vascular degeneration.[23] We quantified this decrease in microvascular tortuosity by measuring a decrease in average vessel length in the DCP. The average vessel length in the SVP + ICP underwent a slight increase throughout the disease process, likely explained by the loss of smaller/shorter capillaries and the retention of the longer arterioles and venules.

There is also some controversy regarding the causative role of the vascular component in the pathophysiology of IRDs. Some groups have suggested that there are early primary vascular changes as part of a systemic "vascular dysregulation syndrome" that are responsible for the vascular spasm and attenuation that would then cause further outer retinal hypoxia and thinning.[17,18] However, the most accepted hypothesis is that the decrease in retinal vascular perfusion is secondary to outer retinal degeneration in response to the drastic drop in metabolic demand.[57–59] Together with the choroidal vascularization, the DCP is known to nourish the outer retina.[60] Hence, it is thought that the primary loss of photoreceptors that occurs in most forms of IRD reduces the metabolic needs of the outer retina, resulting in a secondary vascular remodeling and attenuation that occurs initially in the DCP before affecting the other retinal vascular plexuses. This hypothesis is further supported by our results in two canine models of progressive retinal degeneration that confirmed that the vessel density in the DCP is affected early after the onset of ONL loss. We also showed that in these naturally occurring diseases as well as in a light-induced model of acute photoreceptor degeneration, the DCP is affected earlier than the other retina vascular plexuses. The subsequent decrease in vessel density in the SVP + ICP that occurs in late stages of degeneration is likely a response to the marked outer retinal thinning and the ability for the oxygen transported by choroidal vessels to reach inner retinal locations, because it has been previously confirmed in feline animal models using spatial profiles of retinal oxygenation.[14]

Retinal histopathological studies from laboratory animals and human IRD patient eyes at advanced stages of degeneration show that in areas devoid of photoreceptors, there is RPE cell migration around the inner retinal vessels,[50] where they produce an extracellular matrix, considered to be an ectopic Bruch's membrane, that thickens vessel walls, causing progressive narrowing and occlusion of their lumen.[8,50,61,62] In RP patients, this RPE migration into the inner retina is responsible for the characteristic "bone spicule" pigment formation visible clinically in the fundus. Even though canine models have been extensively used for the development of novel therapies, no studies have specifically evaluated the microscopic vascular changes that occur with retinal degeneration in this species, and it was not known whether the RPE is involved in these changes.

In retinal flat mounts, we observed that the DCP undergoes progressive narrowing and loss of vessels with no overt thickening of their walls. In contrast, the changes in the SVP involved perivascular material deposition that caused apparent narrowing with sporadic occlusion and, in end stages, formation of abnormal vascular complexes in association with translocated RPE cells. Although some of

these changes have been previously described in human and laboratory animal retinas, previous studies did not locate each alteration into specific vascular plexuses.[8,50,61] Here, we have characterized two different types of vascular alterations occurring in the SVP and DCP retinal plexuses over time. Our results suggest that an early vasoconstriction of retinal vessels in the DCP that may be a response to the hyperoxic environment caused by the loss of energy-demanding photoreceptors. At later stages, retinal remodeling including the migration of RPE cells around retinal vessels may cause further constriction and complete occlusion of the vasculature, possibly preventing perfusion of the inner retina and leading to complete retinal atrophy.

The abnormal vascular structures that we identified in the retinal flat mounts in the SVP have been previously reported in laboratory animals as "vascular complexes," where pigmented cells aggregate around capillaries.[23,63–66] To the best of our knowledge, these structures have not been described in canine retinas, and their association with retinal degeneration remains to be elucidated. Importantly, we show that intraretinal migration of RPE cells around inner retinal vessels that lead to the ophthalmoscopic finding described as "bone spicules" in RP patients also occurs in dogs and likely plays a critical role in vascular regression. The lack of pigmentation of RPE cells in the tapetal fundus may explain why this migration of RPE cells that cannot be clinically detected ophthalmoscopically may have been overlooked in dogs. Although a previous histological study described the migration of pigments around canine peripheral blood vessels in areas where the retina was degenerated, thorough characterization or specific labeling confirming their RPE cellular nature was not performed and "vascular complexes" were not identified.[67] In summary, our histopathological findings establish for the first time that RPE migration, similar to that described in RP patients with "bone spicules," also occurs in canine retinas and contributes to the late-stage vascular alterations.[8,50,62]

The acute retinal degeneration that can be experimentally induced in RHO$^{T4R/+}$ dogs exposed to light[42] enabled us to examine the time course and association of retinal vessel abnormalities with the disease. In the naturally occurring models, disease is comparably slower, and vascular changes follow the time course of photoreceptor degeneration. With the light damage model, however, we now show that the vascular changes can occur as early as two weeks after this severe retinal degeneration is triggered. We observed that there was vascular attenuation mainly in the DCP. This further expands the value of this large animal model of inducible retinal degeneration because it could be used to characterize the specific molecular events involved in these early vascular changes over the course of a short time-widow.

Gene therapy in the crd2/*NPHP5* model is able to rescue the structure and restore the function of the photoreceptors,[40] and in this study we observed that it also preserved the vessel density in both vascular plexuses when qualitatively comparing them to the contralateral balanced salt solution–injected eye. It is important to highlight that baseline vascular structural data before the animal was injected was lacking, thus preventing us from drawing conclusions regarding the ability of GT to improve rather than just maintain the structural integrity of the retinal vasculature that is present at the time of intervention.

Biological markers of retinal degeneration are critical for the accurate assessment of the degenerative status of the retina, which in turn defines the therapeutic window when the patients would benefit most from established and newly developed therapies.[6] The number and quality of the retinal vessels is strongly dependent on the metabolic demands of a particular tissue[68,69]; therefore we propose that a significant decrease in vessel density in the DCP could be a good indirect indicator that the metabolic activity in the outer retina is impaired. Hence, characterization of the retinal vascular degenerative state of the DCP might help in the diagnostic, prognostic, and potential therapeutic directions by combining this biomarker with others that assess photoreceptors structural integrity.[70] Additionally, using the vessel density in the DCP as a biomarker will be particularly relevant in experimental regenerative therapies to investigate what are the implications of transplanting photoreceptors in retinas at different stages of vascular regression and how this may favor or limit donor cell survival and integration.

Disclosure: **A. Ripolles-Garcia**, None; **Y. Chen**, None; **Y. Sato**, None; **A. Gray**, None; **G.-S. Ying**, None; **G.D. Aguirre**, None; **W.A. Beltran**, None

References

1. Miyadera K, Acland GM, Aguirre GD. Genetic and phenotypic variations of inherited retinal diseases in dogs: the power of within- and across-breed studies. *Mamm Genome*. 2012;23:40–61.

2. Downs LM, Scott EM, Cideciyan AV, et al. Overlap of abnormal photoreceptor development and progressive degeneration in Leber congenital amaurosis caused by NPHP5 mutation. *Hum Mol Genet*. 2016;25:4211–4226.

3. Suber ML, Pittler SJ, Qin N, et al. Irish setter dogs affected with rod/cone dysplasia contain a nonsense mutation in the rod cGMP phosphodiesterase beta-subunit gene. *Proc Natl Acad Sci USA*. 1993;90:3968–3972.

4. Kijas JW, Cideciyan AV, Aleman TS, et al. Naturally occurring rhodopsin mutation in the dog causes retinal dysfunction and degeneration mimicking human dominant retinitis pigmentosa. *Proc Natl Acad Sci USA*. 2002;99:6328–6333.

5. Zhang Q, Acland GM, Wu WX, et al. Different RPGR exon ORF15 mutations in Canids provide insights into photoreceptor cell degeneration. *Hum Mol Genet*. 2002;11:993–1003.

6. Duncan JL, Pierce EA, Laster AM, et al. Inherited retinal degenerations: current landscape and knowledge gaps. *Transl Vis Sci Technol*. 2018;7:6.

7. Akyol N, Kükner S, Celiker U, Koyu H, Lüleci C. Decreased retinal blood flow in retinitis pigmentosa. *Can J Ophthalmol*. 1995;30:28–32.

8. Milam AH, Li ZY, Fariss RN. Histopathology of the human retina in retinitis pigmentosa. *Prog Retin Eye Res*. 1998;17:175–205.

9. Yu DY, Cringle SJ. Oxygen distribution and consumption within the retina in vascularised and avascular retinas and

in animal models of retinal disease. *Prog Retin Eye Res*. 2001;20:175–208.

10. Yu DY, Cringle SJ, Alder VA, Su EN. Intraretinal oxygen distribution in rats as a function of systemic blood pressure. *Am J Physiol*. 1994;267:H2498–2507.

11. Country MW. Retinal metabolism: a comparative look at energetics in the retina. *Brain Res*. 2017;1672:50–57.

12. Linsenmeier RA, Zhang HF. Retinal oxygen: from animals to humans. *Prog Retin Eye Res*. 2017;58:115–151.

13. Cringle SJ, Yu DY. A multi-layer model of retinal oxygen supply and consumption helps explain the muted rise in inner retinal PO(2) during systemic hyperoxia. *Comp Biochem Physiol A Mol Integr Physiol*. 2002;132:61–66.

14. Padnick-Silver L, Kang Derwent JJ, Giuliano E, Narfström K, Linsenmeier RA. Retinal oxygenation and oxygen metabolism in Abyssinian cats with a hereditary retinal degeneration. *Invest Ophthalmol Vis Sci*. 2006;47:3683–3689.

15. Della Volpe Waizel M, Scholl HPN, Todorova MG. Microvascular and metabolic alterations in retinitis pigmentosa and Stargardt disease. *Acta Ophthalmol*. 2021;99:e1396–e1404.

16. Eysteinsson T, Hardarson SH, Bragason D, Stefánsson E. Retinal vessel oxygen saturation and vessel diameter in retinitis pigmentosa. *Acta Ophthalmol*. 2014;92:449–453.

17. Konieczka K, Flammer AJ, Todorova M, Meyer P, Flammer J. Retinitis pigmentosa and ocular blood flow. *The EPMA Journal*. 2012;3:1–13.

18. Cellini M, Strobbe E, Gizzi C, Campos EC. ET-1 plasma levels and ocular blood flow in retinitis pigmentosa. *Can J Physiol Pharmacol*. 2010;88:630–635.

19. Corazza P, Cirafici P, Testa V, et al. Vascular density and retinal function in patients with retinitis pigmentosa evaluated by swept-source OCT angiography and microperimetry. *Ophthalmologica*. 2021;244:27–33.

20. Hagag AM, Wang J, Lu K, et al. Projection-resolved optical coherence tomographic angiography of retinal plexuses in retinitis pigmentosa. *Am J Ophthalmol*. 2019;204:70–79.

21. Battaglia Parodi M, Cicinelli MV, Rabiolo A, et al. Vessel density analysis in patients with retinitis pigmentosa by means of optical coherence tomography angiography. *Br J Ophthalmol*. 2017;101:428–432.

22. Alnawaiseh M, Schubert F, Heiduschka P, Eter N. Optical coherence tomography angiography in patients with retinitis pigmentosa. *Retina*. 2019;39:210–217.

23. Fernández-Sánchez L, Esquiva G, Pinilla I, Lax P, Cuenca N. Retinal vascular degeneration in the transgenic P23H Rat Model of Retinitis Pigmentosa. *Front Neuroanat*. 2018;12:1–14.

24. Falfoul Y, Elleuch I, El Matri K, et al. Multimodal imaging in retinitis pigmentosa: correlations among microvascular changes, macular function and retinal structure. *J Curr Ophthalmol*. 2020;32:170–177.

25. Ripolles-Garcia A, Ruthel G, Ying G-S, et al. Characterization of the canine retinal vasculature with optical coherence tomography angiography: comparisons with histology and fluorescein angiography. *Front Neuroanat*. 2021;15:1–14.

26. Hormel TT, Jia Y, Jian Y, et al. Plexus-specific retinal vascular anatomy and pathologies as seen by projection-resolved optical coherence tomographic angiography. *Prog Retin Eye Res*. 2021;80:100878.

27. Rezaei KA, Zhang Q, Chen CL, Chao J, Wang RK. Retinal and choroidal vascular features in patients with retinitis pigmentosa imaged by OCT based microangiography. *Graefes Arch Clin Exp Ophthalmol*. 2017;255:1287–1295.

28. Beltran WA, Cideciyan AV, Guziewicz KE, et al. Canine retina has a primate fovea-like bouquet of cone photoreceptors which is affected by inherited macular degenerations. *PLoS One*. 2014;9:e90390.

29. Occelli LM, Pirie CG, SM Petersen-Jones. Non-invasive optical coherence tomography angiography: A comparison with fluorescein and indocyanine green angiography in normal adult dogs and cats. *Vet Ophthalmol*. 2022.

30. Ong SS, Patel TP, Singh MS. Optical coherence tomography angiography imaging in inherited retinal diseases. *J Clin Med*. 2019;8:2078.

31. Jauregui R, Park KS, Duong JK, Mahajan VB, Tsang SH. Quantitative progression of retinitis pigmentosa by optical coherence tomography angiography. *Sci Rep*. 2018;8:1–7.

32. Mastropasqua R, D'Aloisio R, De Nicola C, et al. Widefield Swept Source OCTA in Retinitis Pigmentosa. *Diagnostics (Basel)*. 2020;10:1–13.

33. Kim T-H, Son T, Lu Y, Alam M, Yao X. Comparative Optical Coherence Tomography Angiography of Wild-Type and rd10 Mouse Retinas. *Transl Vis Sci Technol*. 2018;7:42–42.

34. Yilmaz AC, Durukan AH, Yilmaz H, Karaca U. Optical coherence tomography angiography in patients with cone dystrophy. *Semin Ophthalmol*. 2022;37:485–490.

35. AttaAllah HR, Mohamed AAM, Hamid MA. Quantification of macular microvascular changes in retinitis pigmentosa using optical coherence tomography angiography. *Clin Ophthalmol*. 2020;14:1705–1713.

36. Sabbaghi H, Daftarian N, Hassanpour K, et al. Retinal vascular abnormalities in different types of inherited retinal dystrophies assessed by optical coherence tomography angiography. *J Curr Ophthalmol*. 2021;33:189–196.

37. Sugahara M, Miyata M, Ishihara K, et al. Optical coherence tomography angiography to estimate retinal blood flow in eyes with retinitis pigmentosa. *Sci Rep*. 2017;7:46396.

38. Takagi S, Hirami Y, Takahashi M, et al. Optical coherence tomography angiography in patients with retinitis pigmentosa who have normal visual acuity. *Acta Ophthalmol*. 2018;96:e636–e642.

39. Toto L, Borrelli E, Mastropasqua R, et al. Macular features in retinitis pigmentosa: correlations among ganglion cell complex thickness, capillary density, and macular function. *Invest Ophthalmol Vis Sci*. 2016;57:6360–6366.

40. Aguirre GD, Cideciyan AV, Dufour VL, et al. Gene therapy reforms photoreceptor structure and restores vision in NPHP5-associated Leber congenital amaurosis. *Mol Ther*. 2021;29:2456–2468.

41. Cideciyan AV, Sudharsan R, Dufour VL, et al. Mutation-independent rhodopsin gene therapy by knockdown and replacement with a single AAV vector. *Proc Natl Acad Sci USA*. 2018;115:E8547–E8556.

42. Iwabe S, Ying GS, Aguirre GD, Beltran WA. Assessment of visual function and retinal structure following acute light exposure in the light sensitive T4R rhodopsin mutant dog. *Exp Eye Res*. 2016;146:341–353.

43. Zudaire E, Gambardella L, Kurcz C, Vermeren S. A computational tool for quantitative analysis of vascular networks. *PLoS One*. 2011;6:e27385.

44. Wagner DD. Cell biology of von Willebrand factor. *Ann Rev Cell Biol*. 1990;6:217–246.

45. Essner E, Lin WL. Immunocytochemical localization of laminin, type IV collagen and fibronectin in rat retinal vessels. *Exp Eye Res*. 1988;47:317–327.

46. Team RC. R: A language and environment for statistical computing. *Vienna, Austria: R Foundation for Statistical Computing;* 2018: Available online at https://www.R-project.org/.

47. Wickham H. *ggplot2: elegant graphics for data analysis*. Springer; 2016:189–201.

48. Beltran WA, Hammond P, Acland GM, Aguirre GD. A frameshift mutation in RPGR exon ORF15 causes photoreceptor degeneration and inner retina remodeling in a model

of X-linked retinitis pigmentosa. *Invest Ophthalmol Vis Sci*. 2006;47:1669–1681.

49. Berta AI, Boesze-Battaglia K, Genini S, et al. Photoreceptor cell death, proliferation and formation of hybrid rod/S-cone photoreceptors in the degenerating STK38L mutant retina. *PLoS One*. 2011;6:e24074.

50. Li ZY, Possin DE, Milam AH. Histopathology of bone spicule pigmentation in retinitis pigmentosa. *Ophthalmology*. 1995;102:805–816.

51. Arrigo A, Romano F, Albertini G, Aragona E, Bandello F, Battaglia Parodi M. Vascular patterns in retinitis pigmentosa on swept-source optical coherence tomography angiography. *J Clin Med*. 2019;8:1425.

52. Koyanagi Y, Murakami Y, Funatsu J, et al. Optical coherence tomography angiography of the macular microvasculature changes in retinitis pigmentosa. *Acta Ophthalmol*. 2018;96:e59–e67.

53. Alnawaiseh M, Schubert F, Heiduschka P, Eter N. Optical coherence tomography angiography in patients with retinitis pigmentosa. *Retina*. 2019;39:210–217.

54. Lei J, Pei C, Wen C, Abdelfattah NS. Repeatability and reproducibility of quantification of superficial peri-papillary capillaries by four different optical coherence tomography angiography devices. *Sci Rep*. 2018;8:17866.

55. Li XX, Wu W, Zhou H, et al. A quantitative comparison of five optical coherence tomography angiography systems in clinical performance. *Int J Ophthalmol*. 2018;11:1784–1795.

56. Munk MR, Giannakaki-Zimmermann H, Berger L, et al. OCT-angiography: A qualitative and quantitative comparison of 4 OCT-A devices. *PLoS One*. 2017;12:e0177059.

57. Stone JL, Barlow WE, Humayun MS, de Juan E, Milam AH. Morphometric analysis of macular photoreceptors and ganglion cells in retinas with retinitis pigmentosa. *Arch Ophthalmol*. 1992;110:1634–1639.

58. Rangaswamy NV, Patel HM, Locke KG, Hood DC, Birch DG. A comparison of visual field sensitivity to photoreceptor thickness in retinitis pigmentosa. *Invest Ophthalmol Vis Sci*. 2010;51:4213–4219.

59. Verbakel SK, van Huet RAC, Boon CJF, et al. Non-syndromic retinitis pigmentosa. *Prog Retin Eye Res*. 2018;66:157–186.

60. Hagag AM, Pechauer AD, Liu L, et al. OCT Angiography Changes in the 3 Parafoveal Retinal Plexuses in Response to Hyperoxia. *Ophthalmol Retina*. 2018;2:329–336.

61. Blanks JC, Johnson LV. Vascular atrophy in the retinal degenerative rd mouse. *J Comp Neurol*. 1986;254:543–553.

62. Newton F, Megaw R. Mechanisms of photoreceptor death in retinitis pigmentosa. *Genes (Basel)*. 2020;11:1–29.

63. Wang S, Villegas-Pérez MP, Holmes T, et al. Evolving neurovascular relationships in the RCS rat with age. *Curr Eye Res*. 2003;27:183–196.

64. Fernández-Sánchez L, Lax P, Campello L, Pinilla I, Cuenca N. Astrocytes and Müller cell alterations during retinal degeneration in a transgenic rat model of retinitis pigmentosa. *Front Cell Neurosci*. 2015;9:484.

65. Bourne MC, Campbell DA, Tansley K. Hereditary degeneration of the rat retina. *Br J Ophthalmol*. 1938;22:613–623.

66. Wang S, Villegas-Pérez MP, Vidal-Sanz M, Lund RD. Progressive optic axon dystrophy and vascular changes in RD mice. *Invest Ophthalmol Vis Sci*. 2000;41:537–545.

67. Slatter DH, Nelson AW, Young S, Stringer JM, Fisher MW. Retinal vessels of canine eyes at different ages—a qualitative and quantitative study. *Exp Eye Res*. 1979;28:369–379.

68. Guyton AC, Carrier O, Walker JR. Evidence for tissue oxygen demand as the major factor causing autoregulation. *Circ Res*. 1964;15(Suppl):60–69.

69. Pournaras CJ, Rungger-Brändle E, Riva CE, Hardarson SH, Stefansson E. Regulation of retinal blood flow in health and disease. *Prog Retin Eye Res*. 2008;27:284–330.

70. Lu BW, Chao GJ, Wu GP, Xie LK. In depth understanding of retinitis pigmentosa pathogenesis through optical coherence tomography angiography analysis: a narrative review. *Int J Ophthalmol*. 2021;14:1979–1985.